JOURNAL OF MATERIALS SCIENCE **40** (2005) 107–110

Studies on the porous scaffold made of the nano-HA/PA66 composite

ZHANG LI, LI YUBAO*, WANG XUEJIANG, WEI JIE, PENG XUELIN
Research Center for Nano-Biomaterials, Analytical and Testing Center, Sichuan University, Chengdu 610064, People's Republic of China
E-mail: nic7504@scu.edu.cn

Porous scaffolds made of *n*-HA/PA66 composite were fabricated through porogen-leaching technique. The structure, phase and morphology of the scaffolds were investigated by using IR, XRD and SEM, and the physical properties were also studied. The results indicated that the two phases in the composite dispersed uniformly and chemical bonding existed between the two phases. The porosity was proportional to the content of the porogen, and macropores and micropores coexisted and interconnected in the scaffolds. When the porosity was up to 80%, the porosity and the mechanical strength of the scaffolds prepared can meet the demands of tissue engineering simultaneously.

1. Introduction

Hydroxyapatite (HA), the main mineral composition of bone, has been wildly used for bone repair and substitute due to its high biocompatible, bioactive and osteoconductive properties [1–3]. However, brittleness and poor mechanical strength, to some extent, inhibit the use of HA in loading-bearing parts of the body [4, 5]. From the view of materials point, bone is a composite of organic and inorganic phases with highly hierarchical structure. Its main building blocks are long collagen fibrils containing poorly crystalline nanosized HA crystals [6]. So a number of studies have recently centered on the potential application of organic and inorganic composite to generate novel tissue engineering constructs. Organic-inorganic composite using the principle of biomineralization has been developed to match natural skeleton and improve structural properties [7–11].

PA66, a kind of engineering polymer materials, has been clinically used because of its good property and biocompatibility. Numerous hydrogen bonds contained in PA66 drive it to crystallize easily and thus endow the polymer with excellent mechanical properties. Meanwhile, PA66 has the specific chemical bonds, such as amide bonds and carboxyl group, similar to those of collagen in bone, so the composite with 40 wt% HA and 60 wt% PA66 prepared in our research group would be expected to be highly biomimetic [12].

Scaffold architectures that encompass unique arrangement and style of structural elements contribute significantly to specific biological functioning by providing organizational and spatial cues toward morphogenesis [13]. So the optimal scaffold not only mimics the three-dimensional structure of porous bone, but also attracts the cells, facilitates adhesion and spreading, and stimulates the cells to produce new bone matrix in response to the mechanical environment [14]. In this study, the porous scaffold made of the *n*-HA/PA66 composite were prepared by the porogen leaching method and the pore structure was fabricated by controlling the property and fraction of the porogen.

2. Materials and methods

At first, the solvent that would be used in the later process in the experiment was prepared by dissolving chlorate into ethanol to get a saturated solution. Using NaCl particles as the porogen in the study, we blended these particles with the above *n*-HA/PA66 composite powders uniformly according to the NaCl/composite weight ratio 1:1, 3:1 and 4:1, respectively. The pre-prepared solvent was poured into the mixture with a constant stirring for 30 min, thus a sticky slurry was obtained and immediately manipulated into plates with the size of $\phi 30 \times 5$ mm. Then, these plates were immersed into deionized water for 72 h to completely remove the solvent and the porogen, and subsequently taken out and dried under a vacuum to form the desired porous scaffold.

The structure of the scaffold was observed by scanning electron microscopy (SEM). The crystal phase of the material was examined by XRD and IR before and after dissolving in the solvent. In addition, the compressive strength and the porosity of the scaffold were also measured.

*Author to whom all correspondence should be addressed.

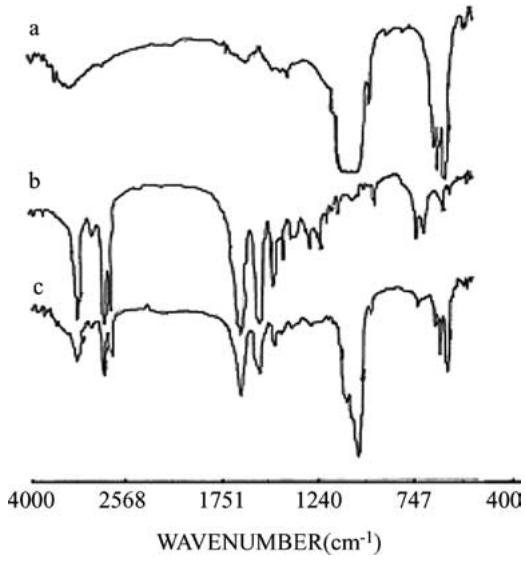

Figure 1 IR spectra of *n*-HA, PA66 and *n*-HA/PA66 composite: (a) *n*-HA prepared by hydrothermal method, (b) PA66, and (c) *n*-HA/PA66 composite.

3. Results and discussion

3.1. IR and XRD analyses of the starting composite

The IR spectra of *n*-HA, PA66 and *n*-HA/PA66 composite are present in Fig. 1. Fig. 1a is that for *n*-HA, b is for PA66 and c is for the composite. In the Fig. 1a, the two bands at 3572 cm^{-1} and 631 cm^{-1} belong to the vibration of hydroxyl group; the band at 962 cm^{-1} is the characteristic band of phosphate stretching vibration, while the band at 1430 cm^{-1} is attributed to the carbonate group. The bands at 1640 and 1538 cm^{-1} in Fig. 1b are the characteristic bands of amide. By analogy with the IR spectra of *n*-HA and PA66 standard samples, we can see that the composite (Fig. 1c) is characterized by absorption bands arising from *n*-HA and PA66, which indicate that no marked changes have taken place in the chemical components of the composite. However, some minute changes can be still observed from these patterns, which shows that some interactions could happen between the *n*-HA and PA66 when they were hybridized. These interactions might be attributed to the hydrogen bonds formed between the ─NH─ and ─C═O─ groups of PA66 and the ─OH of *n*-HA as well as the chemical bonds arising from the attraction between the cation (Ca^{2+}) and the anion ($─COO^{-}$). Besides, *n*-HA particles might enter into the networks of PA66 fibrils and destroy the linkage between the chains in PA66, thus decrease the concentration of hydrogen bonds, which might be another reason to explain the effects between the two components. It is just these interactions that enhance the interfacial action and make the two phases disperse into each other uniformly.

Many tests have shown that there are no new bone formation in highly crystalline porous HA ceramics, but bone generation has been observed in poorly crystalline HA ceramics [15–18]. Therefore, using the poorly crystalline nanosized HA should significantly increase the bioactivity of the composite, which, in turn, could lead to the faster establishment of a strong bond between the composite and tissue. While the PA66 phase will provide the composite with advantage to benefit bone remodeling in human body.

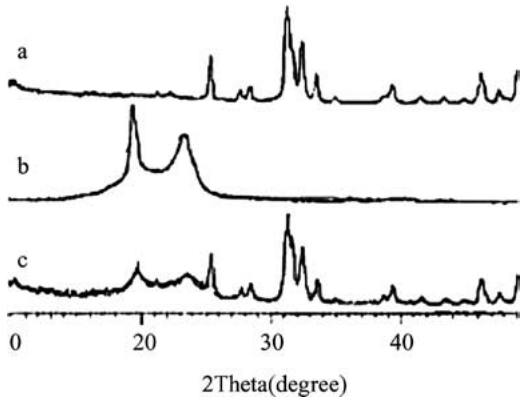

Figure 2 XRD patterns of *n*-HA, PA66 and *n*-HA/PA66 composite: (a) *n*-HA prepared by hydrothermal method, (b) PA66, and (c) *n*-HA/PA66 composite.

In Fig. 2, it can be seen that the crystallization and structure of *n*-HA did not change significantly and still remained the state of poor crystallization before and after being compounded. However, the peak intensity of PA66 decreased much after being compounded, which might result from the effects of *n*-HA crystals on the density of hydrogen bonds in PA66 and the stronger bond formed between *n*-HA and PA66. This result was in agreement with the analysis of IR.

3.2. Phase changes of the dissolved composite

When the *n*-HA/PA66 composite powder was dissolved in the ethanol solution, whether the crystallization of PA66 has changed or not is an urgent issue to be resolved, so the composite was examined before and after dissolving in the solvent by IR and XRD methods, respectively. Fig. 3a is referred to the composite powder, Fig. 3b is for the dissolved composite pre-hardened in air and Fig. 3c is for the dissolved composite pre-hardened in water. The band

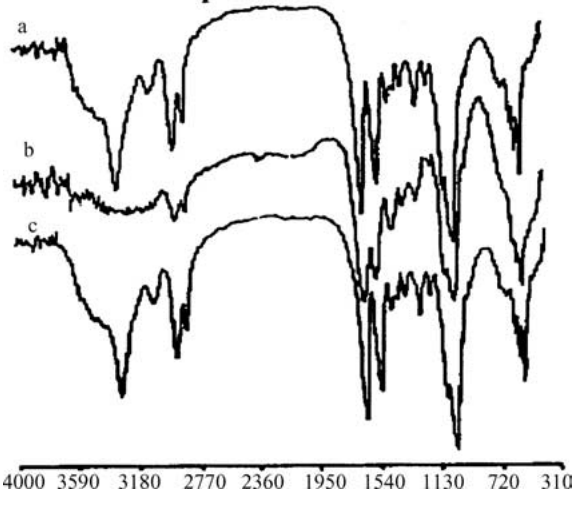

Figure 3 IR spectra of the composite: (a) the starting *n*-HA/PA66 composite, (b) pre-hardened *n*-HA/PA66 in air, and (c) pre-hardened *n*-HA/PA66 in water.

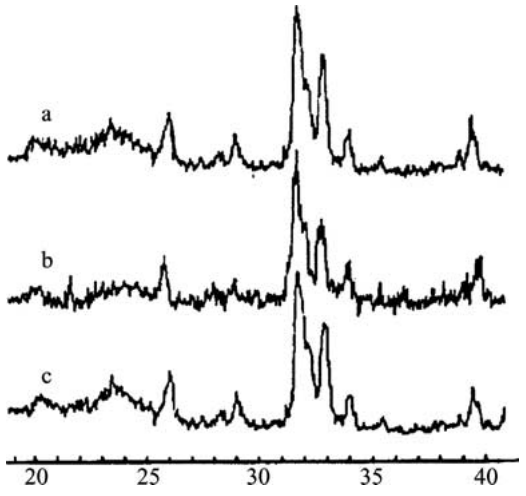

Figure 4 XRD patterns of the composite: (a) the starting *n*-HA/PA66 composite, (b) pre-hardened *n*-HA/PA66 in air and (c) pre-hardened *n*-HA/PA66 in water.

at 3304 cm^{-1} was attributed to the N–H stretching vibration and the band at 690 cm^{-1} was to the N–H bending vibration in Fig. 3a and c. The two bands were observed to completely disappear from the spectra shown in Fig. 3b. The other bands at 1640, 2935, 2861 and 1539 cm^{-1} also simultaneously emerged in Fig. 3a and c. Among these bands, the former was assigned to the –C=O– group, the following two bands to the CH_2 stretching vibration and the latter to the amide II band (N–H and –C=O stretching vibration). These results showed that the IR spectra of *n*-HA/PA66 composite powder was almost the same as that of the dissolved composite pre-hardened in water.

The XRD patterns corresponding to the three samples mentioned above were shown in Fig. 4. As we know, the two peaks at $2\theta = 19.8^\circ$ and 23.8° are the characteristic peaks of crystalline PA66. In the composite powder still showed the two characteristic peaks (Fig. 4a) which disappeared in the XRD pattern of the composite pre-hardened in air (Fig. 4b). When the dissolved composite was placed in water for 72 h, however, the two characteristic peaks appeared again, and their intensity were equal to those of the bands in composite powder shown in Fig. 4a. The results from XRD analysis were also in line with the IR results.

PA66 is a kind of highly crystalline polymer that is hard to be dissolved by most of inorganic or/and organic solvents. In this study, we dissolved the composite in chlorate ethanol solution, which might be due to the chelate reaction between the chlorate and ethanol. We could deduce that the formed chelate complex broke into the chains of PA66 and destroyed the connection of hydrogen bonds, and thus led to the crystallization decrease dramatically. In other words, PA66 in the composite changed from crystalline phase to amorphous phase after dissolving in the solvent. We know that water is the precipitant for PA66, therefore, when the dissolved PA66 was poured into water, precipitates were formed immediately. During the immersion, the ethanol and chlorate in the precipitates could release into water, and the solvent was got rid of as much as possible with the immersion time increasing. With the solvent being eliminated little by little, the polymer transformed from amorphous phase to crystalline phase again, which was determined by the IR and XRD analysis.

3.3. Structural observation

The SEM images of the porous scaffold with an 80% porosity were shown in Fig. 5. A honeycombed structure of the scaffold was observed from Fig. 5a together with good interconnections between the pores. There was a large distribution in pore size for the scaffold with the largest pores greater than 400 μm, mainly in the range of 100–400 μm, and the smaller pores could also be seen in the size of about 10–50 μm (Fig. 5b), while in the walls of the macropores existed uniformly numerous micropores whose sizes were less than 10 μm (Fig. 5c). To some extent, the porous structure of the prepared scaffold was closely similar to the natural bone burned off the organics [13, 19].

A number of tests have demonstrated that bone cells are sensitive to the physical properties of their immediate environment with surface composition, roughness and topography all contributing to the osteogenic process [13, 20, 21]. Surface topography and roughness in particular, as opposed to the design of implant shape, are key determinants in cell contact, growth and osteointegration. Rough surfaces promote bone formation through increased osteoblast attachment, and grooved

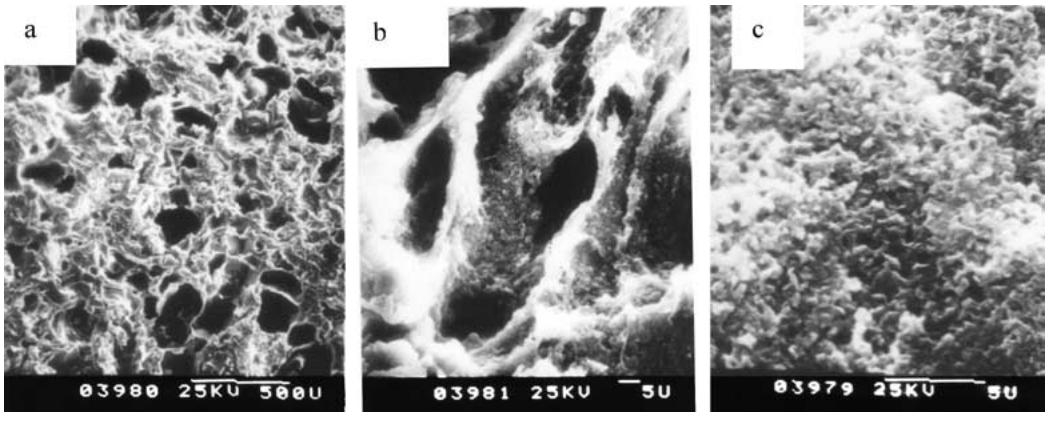

Figure 5 SEM photos of the *n*-HA/PA66 scaffold with 80% porosity: (a) macropores (b) and (c) micropores.

TABLE I The relationship between the porosity and the compressive strength

Porogen/composite (w/w)	Porosity (%)	Compressive strength (MPa)
1:1	37.0	31.00
3:1	65.5	15.2
4:1	85.0	8.70

and microtextured surfaces modulate osteoblast differentiation and function. Osteoblasts also respond directly to the pore dimensions and interconnectivity of scaffold frameworks. Experiments have expressed that micropores (diameter <50 μm) allow blood capillaries to grow in and facilitate nutrients transportation and osteogenic factors reservation, while pores with 100–500 μm diameter permit bone to grow into implants and it would be necessary to ensure rapid colonization of the implant with blood vessels and bone cells. In this sense, the prepared scaffold has the characteristic structure and topography described as above and can meet the requirement of tissue engineering.

3.4. Physical properties

Porogen content was closely connective to the porosity and compressive strength of the prepared scaffold, which was shown in Table I. From the data we could conclude that the porosity was proportional to the porogen contents, while the compressive strength was the inverse.

Scaffolds using in bone tissue engineering are demanded to be able to bear loadings during the process of osteoblast growth, proliferation and differentiation. So there is a clear requirement for the important materials to be mechanically appropriate to their environment, and thus provide and maintain the space for bone cell growth. Although macroporosity facilitates bone formation, it simultaneously decreases the compressive strength of scaffold [20, 21]. Therefore, it is necessary to design an appropriate architecture of the scaffold to meet both the biological and the mechanical requirements that depend on the application.

In the case of scaffolds using in tissue engineering, the porosity should be no less than 75%. The prepared scaffold in this study had the porosity up to 85% and its compressive strength reached about 9 MPa when the weight ratio of NaCl/composite was 4:1. With the similar porosity, however, the compressive strength of the scaffold made of PLA/β-TCP composite was only 1.69 MPa. The difference could be attributed to a magnitude of hydrogen bonds existing between the chains of PA66 which make the polymer be ready to crystallize and consequently provide its products with high mechanical strength. In the composite, organic phase (PA66) decreased the brittleness of HA, and the inorganic nanosized bioactive HA particles, in turn, strengthened the organic phase through the particulate dispersing effects, which led to the higher mechanical strength of amide composite than that of PLA composite. Consequently, the porous materials prepared in this study could be well content with both the mechanical and morphological requirements for the scaffold using in tissue engineering.

4. Conclusions

In this paper, the prepared scaffold made of *n*-HA/PA66 composite has high biomimetic and mechanical properties as well as appropriate porosity and morphology, so it could be expected to be used as scaffold material in bone repair and bone tissue engineering.

Acknowledgement

This study was funded by the Ministry of Science and Technology of China.

References

1. LI YUBAO, J. DE WIJN, C. P. A. T. KLEIN, S. VAN DE MEER and K. DE GROOT, *J. Mater. Sci. Mater. Med.* **5** (1995) 252.
2. SYLVAIN BOHIC, DOMINIQUE HEYMANN, JEAN ALBERT POUEZAT, OLIVIER GAUTHIER and GUY DACULSI, *Life Sci.* **321** (1998) 865.
3. K. D. ROGERS and P. DANIELS, *Biomaterials* **23** (2002) 2577.
4. LI YUBAO, C. P. A. T. KLEIN, J. DE WIJN, S. VAN DE MEER and K. DE GROOT, *J. Mater. Sci. Mater. Med.* **5** (1994) 263.
5. LI YUBAO, ZHANG XINGDONG and K. DE GROOT, *Biomaterials* **18** (1997) 737.
6. X. SU, K. SUN, F. Z. CUI and W. J. LANDIS, *Bone.* **32** (2003) 150.
7. T. H. ANG, F. S. A. SULTANA, D. W. HUTMACHER and Y. S. WONG, *et al.*, *Mater. Sci. Eng.* **20** (2002) 35.
8. S. VIALA, M. FRECHE and J. L. LACOUT, *Ann. Chim. Sci. Mat.* **23** (1998) 67.
9. MYUNG CHUL CHANG and JUNZO TANAKA, *Biomaterials* **23** (2002) 4811.
10. FEI CHEN, ZHOU-CHENG WANG and CHANG-JIAN LIN, *Mater. Lett.* **57** (2002) 858.
11. D. BAKOS, M. SOLDAN and I. HERNANDEZ-FUENTES, *Biomaterials* **20** (1999) 191.
12. XUEJIANG WANG, YUBAO LI, JIE WEI and K. DE GROOT, *ibid.* **23** (2002) 4787.
13. D. GREEN, D. WALSH, S. MANN and R. O. C. OREFFO, *Bone.* **30** (2002) 810.
14. YING YANG, JULIA L. MAGNAY, LEANNE COOLING and ALICIA J. EL HAJ, *Biomaterials* **23** (2002) 2119.
15. A. CUNEYT TAS, *ibid.* **21** (2000) 1429
16. JIAN DONG, TOSHIMASA and HIROKO KOJIMA, *et al.*, *Mater. Sci. Eng.* **17** (2001) 37.
17. DEFNE BAYRAKTAR and A. CUNEYT TAS, *J. Euro. Ceram. Soci.* **19** (1999) 2573.
18. M. OKAZAKI and J. TAKAHASHI, *Biomaterials* **20** (1999) 1073.
19. S. JOSCHEK, B. NIES, R. KROTZ and A. GOPFERICH, *ibid.* **21** (2002) 1645.
20. E. CHARRIERE, J. LEMAITRE and PH. ZYSSET, *ibid.* **24** (2003) 809.
21. JAN WERNER, BRITTA LINNER-KRCMAR, WOLFGANG FRIESS and PETER GREIL, *ibid.* **23** (2002) 4285.

Received 29 December
and accepted 18 August 2004